

# Uncertainty-aware Test-Time Training (UT<sup>3</sup>) for Efficient On-the-fly Domain Adaptive Dense Regression

Uddeshya Upadhyay

## Abstract

Deep neural networks (DNNs) are increasingly being used in autonomous systems. However, DNNs do not generalize well to domain shift. Adapting to a continuously evolving environment is a safety-critical challenge inevitably faced by all autonomous systems deployed to the real world. Recent work on test-time training proposes methods that adapt to a new test distribution on the fly by optimizing the DNN model for each test input using self-supervision. However, these techniques result in a sharp increase in inference time as multiple forward and backward passes are required for a single test sample (for test-time training) before finally making the prediction based on the fine-tuned features. This is undesirable for real-world robotics applications where these models may be deployed to resource constraint hardware with strong latency requirements. In this work, we propose a new framework (called UT<sup>3</sup>) that leverages test-time training for improved performance in the presence of continuous domain shift while also decreasing the inference time, making it suitable for real-world applications. Our method proposes an uncertainty-aware self-supervision task for efficient test-time training that leverages the quantified uncertainty to selectively apply the training leading to sharp improvements in the inference time while performing comparably to standard test-time training protocol. Our proposed protocol offers a continuous setting to identify the selected keyframes, allowing the end-user to control how often to apply test-time training. We demonstrate the efficacy of our method on a dense regression task – monocular depth estimation. Our experiments show that the standard test-time training technique can be made more efficient via multiple strategies for continuous domain adaptation, and our proposed method, UT<sup>3</sup>, is the fastest (i.e., more efficient) among all methods in the presence of test data from shifted domain.

## 1 Introduction

Recent advances in deep learning have enabled a new generation of autonomous agents that can operate in the real world. These advances were primarily driven by deep learning techniques that have led to breakthroughs for tasks like semantic segmentation (Chen et al., 2017), monocular depth estimation (Godard et al., 2019), and other image-based tasks. However, while opening new avenues for autonomous agents in the real world, deep learning is often brittle to even subtle domain shifts. This raises important questions about the reliability and safety of these systems and constitutes a significant obstacle to deploying these systems at scale. This brittleness of deep predictors can be explained by the phenomenon of covariate shift: when deployed to the real world, the data distribution gradually shifts away from the distribution the neural network was trained on, leading to undefined behavior. While the problem could be alleviated through periodic retraining, this solution is time-consuming and expensive in both compute and annotation costs. An alternative is given by domain adaptation (Bridle & Cox, 1990; Ben-David et al., 2010), where the model is trained with labeled data from a source domain and an unlabeled target domain. However, this solution is still inherently offline and does not resolve the problem of covariate shift within a single mission. Recent works tackle the problem of domain adaptation in an online fashion, however, they largely focus on semantic segmentation and/or classification and assume the existence of a class prototype, which is not possible for dense regression. Also, they often require a replay buffer consisting of samples from the training set that increases the resource requirements for the autonomous system that it is deployed on (Panagiotakopoulos et al., 2022; Wang et al., 2022; Iwasawa & Matsuo, 2021; Liu et al., 2023).

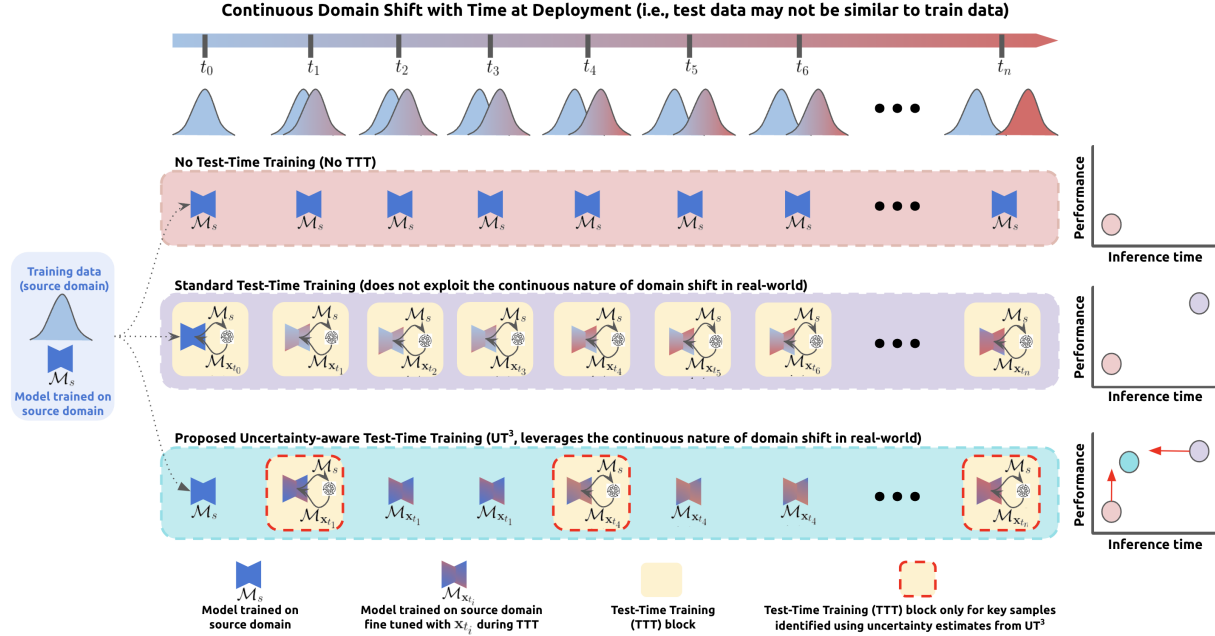


**Figure 1:** In the presence of a continuously drifting domain: (Top) Using a fixed model leads to poor performance. (Middle) Using *test-time training* leads to improved performance but at higher inference time, limiting real-world use cases. (Bottom) Using *uncertainty-aware test-time training* ( $UT^3$ ) leads to improved performance and reduced inference time, making it applicable to real-world settings.

Recently, Test-Time-Training (TTT) (Sun et al., 2020) was proposed as a promising alternative to offline domain adaptation. Test-time training applies a few training steps to the network for each new input using a self-supervised training objective. As was shown by Sun et al. (2020), this technique makes neural networks significantly more robust for classification tasks. Since its first introduction, multiple self-supervised training objectives have been proposed for test-time training, including entropy minimization (Wang et al., 2020a) and masked autoencoders (Gandelsman et al., 2022). However, all these techniques have in common that they need to apply multiple training steps (e.g. 30) to each new example at test time, leading to a significant test-time overhead. In this paper, we address this challenge. Our key insight is that the test-time overhead can be significantly ameliorated by leveraging advances in uncertainty estimation (Kendall & Gal, 2017; Upadhyay et al., 2022) for deep neural predictors and by exploiting the continuity of the covariate shift over time. This is visualized in Fig. 1: instead of retraining the network from scratch for every test sample, we propose to intelligently select keyframes, to which we apply test-time-training and preserve the state of the DNNs, till we hit the next keyframe. We select these keyframes using uncertainty estimates and name our approach *Uncertainty-Aware Test-Time Training* ( $UT^3$ ). In addition, we propose a novel uncertainty-aware self-supervised training objective for test-time training of monocular depth estimation and show that test-time training can be effectively applied to a regression problem. In contrast to classification and segmentation tasks that were studied before, for depth estimation, we can exploit structural knowledge about the 3D world and build on existing self-supervised training objectives for offline training (Godard et al., 2019).

In summary, our contributions are as follows: (i) We show how test-time training can be made more efficient by intelligently selecting keyframes (using uncertainty estimation) and preserving the context between keyframes. (ii) We show that test-time training can be effectively applied to dense regression tasks like monocular depth estimation. (iii) We propose a novel uncertainty-aware self-supervised training objective for test-time training of monocular depth estimation. (iv) We provide experimental insights into the advantages and disadvantages of different variants of test-time training for continuous sequences.

## 2 Related Work

**Monocular Depth Estimation.** Scene depth estimation is an important task in computer vision, which enhances the perception and understanding of real three-dimensional scenes leading to a wide range of

applications such as robotic navigation, autonomous driving, and virtual reality (Ming et al., 2021; El Jamiy & Marsh, 2019; Ye et al., 2017). Depth estimation can be broadly classified into (i) active depth estimation and (ii) image-based depth estimation. Active depth estimation leverages lasers, structured light, and other reflections on the object surface to obtain depth point clouds, complete surface modeling, and estimate scene depth maps (Ming et al., 2021; Kumar et al., 2018; Park et al., 2019) but these methods involve heavy costs of data preparation, labeling, and computing resources (Ming et al., 2021). Image-based depth estimations are more attractive as they cut the need for heavy resources while being applicable to a wide range of applications (Godard et al., 2019; 2017; Fu et al., 2018; Hong et al., 2022). However, most of these work train models once with a fixed dataset before real-world deployment, which is bound to fail in a continuously evolving environment that may drift away from the training dataset. Hence, an efficient online domain adaptive technique is essential to make these methods more robust.

**Domain Adaptation.** As discussed above, a significant challenge with machine learning methods that are deployed to the real world is the drift in the input domain at the test time (i.e., the target domain may not be similar to the source domain). Domain adaptation techniques transfer knowledge from a source domain to a target domain. This has been widely studied in various applications, including computer vision (Wang & Deng, 2018; Csurka, 2017), natural language processing (Jiang & Zhai, 2007; Ramponi & Plank, 2020; Blitzer et al., 2006), and speech recognition (Deng et al., 2017; Latif et al., 2022). One well-studied approach for domain adaptation is the use of domain-invariant features (Fernando et al., 2013), which aims to align the source and target domains by learning representations that are invariant to the domain shift. This has been further extended to adversarial learning (Ganin et al., 2016), where a discriminator is trained to distinguish between the source and target domains while the feature extractor tries to fool the discriminator. Another popular approach is to use instance-level adaptation (Zhang et al., 2021; Liu et al., 2020), where samples from the target domain are re-weighted based on their similarity to source domain samples. This has been shown to be effective in scenarios where the target domain has limited annotated data. Other works like (Mansour et al., 2008; Wang et al., 2020b; Sun et al., 2015) have also explored combining multiple domains, where the goal is to leverage the information from multiple domains to improve the adaptation performance. This has been shown to be particularly effective in scenarios where the source domains are complementary. However, many previous techniques attempt domain adaptation in an offline fashion, which depends on having certain knowledge about the potentially unseen domain. Works such as (Panagiotakopoulos et al., 2022; Wang et al., 2022; Iwasawa & Matsuo, 2021; Liu et al., 2023) propose an online scheme to perform domain adaptation in the context of semantic segmentation/classification. However, they assume the existence of a class prototype, which is not possible for dense regression.

**Test-Time Training (TTT).** It is a technique where the model is fine-tuned on new data at test time using self-supervision (Sun et al., 2020; Liu et al., 2021). While it attempts to tackle the same problem of domain shift as domain adaptation, the difference is that TTT does not require any information about the potential target SHIFT. During training, unlike domain adaptation. A typical TTT framework consists of a primary-task branch and a self-supervision task branch, both sharing a common encoder. For a sample at test time, first, the encoder and self-supervision head are fine-tuned on the sample. Afterward, the fine-tuned encoder is used with the primary task head to make the final prediction (Lin et al., 2022; Gandselman et al., 2022; Sun et al., 2020). This approach has been shown to be effective for computer vision tasks (Zhou et al., 2022; Koh et al., 2021; Wang et al., 2022; Azimi et al., 2022; Wang et al.; Zhang et al., 2022). However, TTT comes at the cost of higher inference time, making them unsuitable for low-latency, real-world applications.

**Uncertainty Estimation.** It is a crucial task in machine learning, particularly for deep neural networks applied to safety-critical applications (Gal, 2016; Kendall & Gal, 2017; Laves et al., 2020a;b; Sudarshan et al., 2021; Upadhyay et al., 2021a;b;c), as it can allow triggering interventions when the model is not confident in the predictions. Uncertainty estimation can be used for various purposes, such as active learning, model selection, and out-of-distribution detection (Lakshminarayanan et al., 2016; Durasov et al., 2021; Malinin & Gales, 2018; Shapeev et al., 2020; Tian et al., 2020). Another popular approach for uncertainty estimation in deep neural networks is Bayesian deep learning (Wilson & Izmailov, 2020; Wang & Yeung, 2020; Abdullah et al., 2022; Daxberger et al., 2021; Gustafsson et al., 2020). This approach involves modeling the parameters of the network as random variables and estimating their posterior distribution. In this paper, we leverage these advances in uncertainty estimation to reduce latency for test-time training by using these estimates to intelligently apply test-time training.

### 3 Method

Section 3.1 describes the problem formulation. The required preliminaries on test-time training and uncertainty estimation are in Section 3.2.1 and 3.2.2. In Section 3.3, we describe the construction of  $\text{UT}^3$  that proposes an uncertainty-aware test-time training scheme for dense regression tasks (like monocular depth estimation) for efficient test-time training.

#### 3.1 Problem formulation

Let  $\mathcal{D}_s = \{(\mathbf{x}_i, \mathbf{y}_i)\}_{i=1}^N$  be the training set with pairs from domain  $\mathbf{X}_s$  and  $\mathbf{Y}$  (i.e.,  $\mathbf{x}_i \in \mathbf{X}_s, \mathbf{y}_i \in \mathbf{Y}, \forall i$  and  $\mathcal{D}_s$  refers to “source” dataset), where  $\mathbf{X}_s, \mathbf{Y}$  are subsets of  $\mathbb{R}^m$  and  $\mathbb{R}^n$ , respectively. While our formulation is valid for arbitrary dimension, we present the formulation for image-based dense regression task: monocular depth estimation (Godard et al., 2019; 2017; Patil et al., 2022). Therefore,  $(\mathbf{x}_i, \mathbf{y}_i)$  represents a pair of images, where  $\mathbf{x}_i$  refers to the input and  $\mathbf{y}_i$  denotes the corresponding output. For instance, in monocular depth estimation  $\mathbf{x}_i$  is an RGB image, and  $\mathbf{y}_i$  is the depth map for that image. Oftentimes, it is of great interest to learn a deep neural network (DNN),  $\Psi(\cdot; \Theta)$ , that learns a mapping from  $\mathbf{X}_s$  to  $\mathbf{Y}$ , i.e.,  $\Psi(\cdot; \Theta) : \mathbf{X}_s \rightarrow \mathbf{Y}$ . In this work, we examine the problem of making  $\Psi$  generalizable to an arbitrary shifted domain  $\mathbf{X}_t$  (Zhao et al., 2019; Roussel et al., 2019). For instance, depth estimation models for autonomous driving may be trained in a particular environment but should reliably work in novel environments and surroundings (i.e., different weather conditions, lighting, cities, etc.) encountered during deployment.

#### 3.2 Preliminaries

##### 3.2.1 Test-time Training

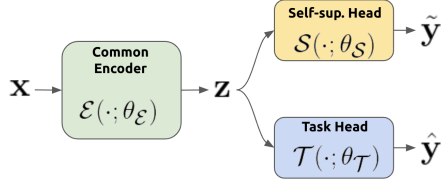


**Figure 2:** The encoder, task-head, and self-supervision head for the test-time training framework.

Recent works (Sun et al., 2020; Gandelsman et al., 2022) have highlighted a general approach for improving the performance of predictive models when training and test data come from different distributions by turning a single unlabeled test sample into a self-supervised learning problem. At each step, the above methods update the model parameters before making a prediction. The approach consists of three crucial components: (i) The common encoder  $\mathcal{E}(\cdot; \theta_{\mathcal{E}})$  that maps an input  $\mathbf{x}$  to a latent representation  $\mathbf{z}$ . (ii) The task dependent head  $\mathcal{T}(\cdot; \theta_{\mathcal{T}})$  that makes the task prediction based on the latent representation  $\mathbf{z}$ . (iii) The self-supervisory head  $\mathcal{S}(\cdot; \theta_{\mathcal{S}})$  that performs a self-supervision task given a latent representation  $\mathbf{z}$ .

The three components are arranged in a Y shape with the encoder feeding into both heads as shown in Figure 2. The parameters for the different modules  $(\{\theta_{\mathcal{E}}^*, \theta_{\mathcal{S}}^*, \theta_{\mathcal{T}}^*\})$  can be obtained by solving the following optimization problem which is a combination of self-supervision and task-dependent objectives as described in (Gandelsman et al., 2022),

$$\{\theta_{\mathcal{E}}^*, \theta_{\mathcal{S}}^*, \theta_{\mathcal{T}}^*\} = \underset{\theta_{\mathcal{E}}, \theta_{\mathcal{S}}, \theta_{\mathcal{T}}}{\operatorname{argmin}} \left[ \underbrace{\lambda_1 \mathcal{L}_{ss}(\mathcal{S}(\mathcal{E}(\mathbf{x}; \theta_{\mathcal{E}}); \theta_{\mathcal{S}}))}_{\text{Self-supervision loss}} + \underbrace{\lambda_2 \mathcal{L}_T(\mathcal{T}(\mathcal{E}(\mathbf{x}; \theta_{\mathcal{E}}); \theta_{\mathcal{T}}), \mathbf{y})}_{\text{Task-dependent loss}} \right] \quad (1)$$

Where,  $(\lambda_1, \lambda_2)$  are hyperparameters controlling the relative contributions of the two losses. While there are other self-supervision techniques for TTT, we use the one described in (Gandelsman et al., 2022) with masked-autoencoders as the self-supervision task leading to a reconstruction based  $\mathcal{L}_{ss}$ , i.e.,  $\mathcal{L}_{ss}(\cdot) = \|\mathcal{S}(\mathcal{E}(\tilde{\mathbf{x}}; \theta_{\mathcal{E}}); \theta_{\mathcal{S}}) - \mathbf{x}\|^2$ . Where  $\tilde{\mathbf{x}} := \text{mask}(\mathbf{x})$  represents the masked input image.  $\mathcal{L}_T$  represents the task-dependent loss term (e.g., cross-entropy for classification). The predictions from the above framework are obtained by a two-step procedure. For a given input  $\mathbf{x}$ , we perform

Step 1 (Test-time Training):  $\theta_{\mathcal{E}, \mathbf{x}}^*, \theta_{\mathcal{S}, \mathbf{x}}^* = \underset{\theta_{\mathcal{E}}, \theta_{\mathcal{S}}}{\operatorname{argmin}} [\mathcal{L}_{ss}(\mathcal{S}(\mathcal{E}(\tilde{\mathbf{x}}; \theta_{\mathcal{E}}); \theta_{\mathcal{S}}))] \text{ with } (\theta_{\mathcal{E}}, \theta_{\mathcal{S}}) \text{ init. to } (\theta_{\mathcal{E}}^*, \theta_{\mathcal{S}}^*) \text{ for } Q \text{ steps}$

Step 2 (Prediction):  $\hat{\mathbf{y}} = \mathcal{T}(\mathcal{E}(\mathbf{x}; \theta_{\mathcal{E}, \mathbf{x}}^*); \theta_{\mathcal{T}}^*)$

### 3.2.2 Uncertainty Estimation

Various works (Gal, 2016; Kendall & Gal, 2017; Lakshminarayanan et al., 2016; Upadhyay et al., 2021a; Laves et al., 2020a; Rangnekar et al., 2023) have proposed different methods to model the uncertainty estimates in the predictions made by DNNs for different tasks. Uncertainty can broadly be categorized into two types (i) aleatoric (uncertainty due to inherent randomness in the data distribution) and (ii) epistemic (uncertainty due to parameters of the model) uncertainty (Gal, 2016; Kendall & Gal, 2017). Interestingly recent works (Kendall & Gal, 2017; Laves et al., 2020a; Upadhyay et al., 2022; 2023a;b;c) have shown that for many real-world computer vision applications with access to large datasets, modeling the aleatoric uncertainty allows for capturing erroneous predictions that may happen with out-of-distribution samples. In the context of regression, this is done by modeling the residual between the prediction and the ground truth as a parametric distribution (often Gaussian) (Kendall & Gal, 2017; Laves et al., 2020a; Sudarshan et al., 2021). Consider a regression DNN model  $\Phi(\cdot; \theta) : \mathbb{R}^m \rightarrow \mathbb{R}^n$ , with a set of trainable parameters given by  $\theta$ . To capture the *irreducible* (i.e., aleatoric) uncertainty in the output distribution  $\mathcal{P}_{Y|X}$ , the model estimates the parameters of the distribution. These are then used to maximize the likelihood function. That is, for an input  $\mathbf{x}_i$ , the model produces a set of parameters representing the output given by,  $\{\hat{\mathbf{y}}_i, \hat{\sigma}_i\} := \Phi(\mathbf{x}_i; \theta)$ , that characterizes the distribution  $\mathcal{P}_{Y|X}(\mathbf{y}; \{\hat{\mathbf{y}}_i, \hat{\sigma}_i\})$ , such that  $\mathbf{y}_i \sim \mathcal{P}_{Y|X}(\mathbf{y}; \{\hat{\mathbf{y}}_i, \hat{\sigma}_i\})$ . The likelihood  $\mathcal{L}(\zeta; \mathcal{D}) := \prod_{i=1}^N \mathcal{P}_{Y|X}(\mathbf{y}_i; \{\hat{\mathbf{y}}_i, \hat{\sigma}_i\})$  is then maximized in order to estimate the optimal parameters of the network. With a *heteroscedastic* Gaussian distribution for  $\mathcal{P}_{Y|X}$  (Kendall & Gal, 2017; Wang et al., 2019), maximizing the likelihood becomes,

$$\theta^* = \underset{\theta}{\operatorname{argmax}} \prod_{i=1}^N \frac{1}{\sqrt{2\pi\hat{\sigma}_i^2}} e^{-\frac{|\hat{\mathbf{y}}_i - \mathbf{y}_i|^2}{2\hat{\sigma}_i^2}} = \underset{\theta}{\operatorname{argmin}} \sum_{i=1}^N \frac{|\hat{\mathbf{y}}_i - \mathbf{y}_i|^2}{2\hat{\sigma}_i^2} + \frac{\log(\hat{\sigma}_i^2)}{2} \quad (2)$$

$$\text{Uncertainty}(\hat{\mathbf{y}}_i) = \hat{\sigma}_i^2. \quad (3)$$

### 3.3 Building UT<sup>3</sup>: Uncertainty-aware Test-Time Training Module

We first consider a framework for the *primary task*. We focus on image-based dense regression, where it is typical to have modules  $\mathcal{E}(\cdot; \theta_E)$  that encodes the input image and  $\mathcal{T}(\cdot; \theta_T)$  that uses the encoded features to synthesize the desired output. To make this framework compatible with test-time training, we notice that we only need to add a self-supervision head  $\mathcal{S}(\cdot; \theta_{SS})$  in the existing framework such that it takes the encodings produced by  $\mathcal{E}$  and performs the self-supervision task. For our experiments, we propose to use a modified uncertainty-aware masked-autoencoding as self-supervision task (Gandelsman et al., 2022; Upadhyay et al., 2022) where the network  $\mathcal{S}(\cdot; \theta_{SS})$  is designed to have a split head to produce a tuple  $(\tilde{\mathbf{y}}, \tilde{\sigma}) := ([\mathcal{S}(\cdot; \theta_{SS})]_{\tilde{\mathbf{y}}}, [\mathcal{S}(\cdot; \theta_{SS})]_{\tilde{\sigma}})$  as described in (Kendall & Gal, 2017; Laves et al., 2020a). Given an input  $\mathbf{x}_i$ , the encoder  $\mathcal{E}$  generates two features: (i)  $\mathcal{E}(\mathbf{x}_i; \theta_E)$ , and (ii)  $\mathcal{E}(\tilde{\mathbf{x}}_i; \theta_E)$ , with  $\tilde{\mathbf{x}}_i = \text{mask}(\mathbf{x}_i)$ . The feature  $\mathcal{E}(\mathbf{x}_i; \theta_E)$  is passed to the primary task head  $\mathcal{T}$  to predict  $\hat{\mathbf{y}}_i := \mathcal{T}(\mathcal{E}(\mathbf{x}_i; \theta_E); \theta_T)$  and the feature  $\mathcal{E}(\tilde{\mathbf{x}}_i; \theta_E)$  is passed to self-supervision head  $\mathcal{S}$  to predict a tuple  $(\tilde{\mathbf{y}}_i, \tilde{\sigma}_i) := ([\mathcal{S}(\mathcal{E}(\tilde{\mathbf{x}}_i; \theta_E); \theta_{SS})]_{\tilde{\mathbf{y}}}, [\mathcal{S}(\mathcal{E}(\tilde{\mathbf{x}}_i; \theta_E); \theta_{SS})]_{\tilde{\sigma}})$ . At training, all the components are trained jointly by optimizing:

$$\{\theta_E^*, \theta_{SS}^*, \theta_T^*\} = \underset{\theta_E, \theta_{SS}, \theta_T}{\operatorname{argmin}} \frac{1}{N} \sum_{i=1}^N \left[ \lambda_1 \underbrace{\mathcal{L}_{uSS}(\mathbf{x}_i, \theta_E, \theta_{SS})}_{\text{Unc. self-sup. loss}} + \lambda_2 \underbrace{\mathcal{L}_T(\mathbf{x}_i, \theta_E, \theta_T, \mathbf{y}_i)}_{\text{Task-dependent loss}} \right] \quad (4)$$

$$\mathcal{L}_{uSS}(\mathbf{x}_i, \theta_E, \theta_{SS}) = \frac{|\mathcal{S}(\mathcal{E}(\tilde{\mathbf{x}}_i; \theta_E); \theta_{SS})]_{\tilde{\mathbf{y}}} - \mathbf{x}_i|^2}{2 [\mathcal{S}(\mathcal{E}(\tilde{\mathbf{x}}_i; \theta_E); \theta_{SS})]_{\tilde{\sigma}}^2} + \frac{\log [\mathcal{S}(\mathcal{E}(\tilde{\mathbf{x}}_i; \theta_E); \theta_{SS})]_{\tilde{\sigma}}^2}{2} \quad (5)$$

In the above,  $\mathcal{L}_{uSS}$  represents the uncertainty-aware self-supervision loss for the masked-autoencoding task. The term  $\mathcal{L}_T$  is the task-dependent supervised loss term discussed in depth in Section 3.4. The above optimization with an initial dataset  $\mathcal{D}_s^{\text{train}} = \{(\mathbf{x}_i, \mathbf{y}_i)\}_{i=1}^N$  leads to an optimal set of parameters  $\{\theta_E^*, \theta_{SS}^*, \theta_T^*\}$ . At test time, for every input sample  $\mathbf{x}$  we first fine-tune the network  $\mathcal{E}(\cdot; \theta_E)$  and  $\mathcal{S}(\cdot; \theta_{SS})$  using the objective function  $\mathcal{L}_{uSS}(\mathbf{x}, \theta_E, \theta_{SS})$  for  $Q$  steps, leading to new set of parameters  $\{\theta_{E,\mathbf{x}}^*, \theta_{SS,\mathbf{x}}^*\}$ . The fine-tuned encoder  $\mathcal{E}(\cdot; \theta_{E,\mathbf{x}}^*)$  is used with the primary task-head  $\mathcal{T}(\cdot; \theta_T^*)$  to make final prediction  $\hat{\mathbf{y}} = \mathcal{T}(\mathcal{E}(\mathbf{x}; \theta_{E,\mathbf{x}}^*); \theta_T^*)$ .

We note that an inherent limitation of standard TTT approach (Gandelsman et al., 2022; Sun et al., 2020) is the time increase to make a prediction: For a test sample, there are  $Q$  forward-backward passes involved,



followed by one final forward pass. One of our key insights is that TTT can be made more efficient for many real-world applications, e.g., monocular depth estimation, by leveraging the fact that test samples are often coming in as a data stream and domain shifts are continuous in nature. That is, the target distribution will not drift drastically over a short period of time. Therefore, it may not be necessary to perform test-time training on every test sample if we are able to identify the few *key* test inputs on which we perform test-time training, and keep the fine-tuned parameters of the following frames (i.e., preserving the states). We propose an entropy-based criterion to identify such key inputs (also called *keyframes*).

For each sample in the validation dataset from the same domain  $\mathcal{D}_s^{\text{val}} = \{(\mathbf{x}_i, \mathbf{y}_i)\}_{i=1}^M$ , we obtain the  $\{\hat{\mathbf{y}}_i, \tilde{\mathbf{y}}_i, \tilde{\sigma}_i\}_{i=1}^M$  and the entropy of the Gaussian distribution predicted by the self-supervision head per sample (parameterized by  $\{\tilde{\mathbf{y}}_i, \tilde{\sigma}_i\}$ , i.e.,  $\mathcal{N}(\tilde{\mathbf{y}}_i, \tilde{\sigma}_i)$ ). The set of all the entropy values for samples in  $\mathcal{D}_s^{\text{val}}$ , say  $\{S_i = \mathcal{H}(\mathcal{N}(\tilde{\mathbf{y}}_i, \tilde{\sigma}_i))\}_{i=1}^M$ , are used to design a threshold given by,

$$\tau_{q,S} = \text{quantile}(\{S_i\}_{i=1}^M, q) \quad (6)$$

Where  $q \in [0, 1]$  controls how high the threshold is. At test time, we perform test-time training for samples whose entropy is greater than  $\tau_{q,S}$ . As we will see later (Section 4.4), this allows us to find the right regime to achieve a target performance with a controlled impact on computational performance. That is, for a given test sample  $\mathbf{x}$  we compute,

$$(\hat{\mathbf{y}}, \tilde{\mathbf{y}}, \tilde{\sigma}) = \left( \mathcal{T}(\mathcal{E}(\mathbf{x}; \theta_E^*); \theta_T^*), [\mathcal{S}(\mathcal{E}(\mathbf{x}; \theta_E^*); \theta_{SS}^*)]_{\tilde{\mathbf{y}}}, [\mathcal{S}(\mathcal{E}(\mathbf{x}; \theta_E^*); \theta_{SS}^*)]_{\tilde{\sigma}} \right) \quad (7)$$

If  $\mathcal{H}(\mathcal{N}(\tilde{\mathbf{y}}, \tilde{\sigma})) > \tau_{q,S}$  we perform test-time training. Otherwise, we use the prediction  $\hat{\mathbf{y}}$  as is.

### 3.4 UT<sup>3</sup> Applied to Monocular Depth Estimation

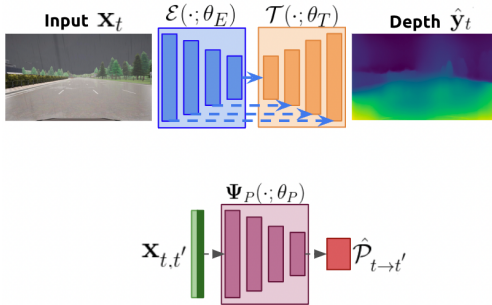


**Figure 3:** Monodepth2 (Godard et al., 2019) components. It consists of an encoder, a decoder, and a pose-estimator.

The work in (Godard et al., 2019) proposed a framework called *MonoDepth2* for monocular depth estimation using deep learning. In addition to our proposed method, a key insight in our work is that we can use the self-supervision loss from Godard et al. (2019) for test-time training without making any changes (detailed in Section 4.1). The framework consists of paired encoder-decoder networks  $\mathcal{E}$  and  $\mathcal{T}$  as shown in Figure 3-(top). In addition to these, there is also a third DNN that estimates the pose estimate between a pair of frames, shown as  $\Psi_P$  in Figure 3-(bottom). The three networks are trained jointly using a combination of photometric projection loss ( $\mathcal{L}_p$ ) and edge-aware smoothing loss ( $\mathcal{L}_s$ ). The loss components are,

$$\mathcal{L}_p = \min_{t'} \left[ \frac{\alpha}{2} (1 - \text{SSIM}(\mathbf{x}_t, \mathbf{x}_{t' \rightarrow t})) + (1 - \alpha) |\mathbf{x}_t - \mathbf{x}_{t' \rightarrow t}| \right] \quad (8)$$

$$\mathcal{L}_s = |\partial_x d_t^*| e^{-|\partial_x \mathbf{x}_t|} + |\partial_y d_t^*| e^{-|\partial_y \mathbf{x}_t|} \quad (9)$$

Where  $\mathbf{x}_{t' \rightarrow t} := \mathbf{x}_{t'} \langle \text{proj}(\hat{\mathbf{y}}_t, \hat{\mathbf{p}}_{t \rightarrow t'}, K) \rangle$  with  $\text{proj}(\cdot)$  are the resulting 2D coordinates of the projected depths  $\hat{\mathbf{y}}_t$  in  $\mathbf{x}_{t'}$ ,  $\langle \cdot \rangle$  is the sampling operator,  $K$  is the intrinsics, and  $d_t^*$  is the mean-normalized inverse depth from (Wang et al., 2018) to discourage shrinking of the estimated depth. The overall objective function for the training is defined by,  $\mathcal{L}_T = \mu_1 \mathcal{L}_p + \mu_2 \mathcal{L}_s$ , where  $(\alpha, \mu_1, \mu_2)$  are set to values as described in (Godard et al., 2019). *MonoDepth2* is trained on the KITTI dataset (Geiger et al., 2012; Godard et al., 2019). To apply our proposed UT<sup>3</sup> framework, we take the pre-trained *MonoDepth2* for monocular depth estimation, i.e., we take  $\mathcal{E}(\cdot; \theta_{E,K_0}^*), \mathcal{T}(\cdot; \theta_{T,K_0}^*), \Psi_P(\cdot; \theta_{P,K_0}^*)$  (where  $\theta_{E/T/P,K_0}^*$  indicates the trained weights) and introduce the masked-autoencoding self-supervision head  $\mathcal{S}(\cdot; \theta_{SS})$ , which is designed similar to  $\mathcal{T}(\cdot; \theta_T)$  except the final layers are split into two estimates the mean and variances of *heteroscedastic* Gaussian as described in Section 3.3. With the addition of the new network, the entire framework is trained again, where we initialize  $\{\theta_E, \theta_T, \theta_P\}$  with the pre-trained weights  $\{\theta_{E,K_0}^*, \theta_{T,K_0}^*, \theta_{P,K_0}^*\}$  and  $\theta_{SS}$  randomly. We train all the networks



**Figure 4:** (Left) Sample from the source domain (KITTI). (Right) Samples from target domains (SHIFT)

jointly on the KITTI dataset by optimizing Equation 4 (described in Section 3.3) with  $\lambda_1 = 1, \lambda_2 = 10^{-3}$  using Adam (Kingma & Ba, 2014) optimizer with an initial learning rate set to  $10^{-5}$  and decayed using cosine annealing. This yields new values for the set of weights  $\{\theta_{E,K_1}^*, \theta_{T,K_1}^*, \theta_{P,K_1}^*, \theta_{SS,K_1}^*\}$ . As described in Section 3.3, we perform test-time training with these weights by fine-tuning the network  $\mathcal{E}(\cdot; \theta_{E,K_1}^*)$  and  $\mathcal{S}(\cdot; \theta_{SS,K_1}^*)$  using the objective function  $\mathcal{L}_{uSS}(\mathbf{x}, \theta_E, \theta_{SS})$  for  $Q$  steps leading to the new set of parameters  $\{\theta_{E,K_1,\mathbf{x}}^*, \theta_{SS,K_1,\mathbf{x}}^*\}$ . The fine-tuned encoder  $\mathcal{E}(\cdot; \theta_{E,K_1,\mathbf{x}}^*)$  is used with the primary task-head  $\mathcal{T}(\cdot; \theta_{T,K_1}^*)$  to make final prediction  $\hat{\mathbf{y}} = \mathcal{T}(\mathcal{E}(\mathbf{x}; \theta_{E,K_1,\mathbf{x}}^*); \theta_{T,K_1}^*)$ .

## 4 Experiments and Results

We provide an overview of the experiments performed and the results obtained. In Section 4.1, we describe the task and various methods used for comparison. Section 4.2 analyzes the phenomena of trained model degrading in the presence of data from shifted domains, highlighting the need for adaptation. Section 4.3 shows that test time training can help significantly improve the performance in the presence of data from continuously shifting domains. We then present the results demonstrating the improved efficiency of test-time-training methods with the help of uncertainty estimation in Section 4.4.

### 4.1 Tasks, Datasets, and Compared Methods

We present the results of all our experiments on the monocular depth estimation task. The base model to perform the task has been trained on the KITTI autonomous driving dataset (Geiger et al., 2012; Godard et al., 2019). To evaluate the performance of various methods in the presence of domain shift, we use the SHIFT dataset (Sun et al., 2022) for autonomous driving which simulates different weather conditions, lighting conditions, cities, etc, as shown in Figure 4. We use *MonoDepth2* (Godard et al., 2019) trained on the KITTI dataset as our base model that performs monocular depth estimation. Following the design principles described in Section 3.2.1, we design various test-time training methods based on *MonoDepth2*: (i) TTT **orig-SS** leverages the existing self-supervision component based on photometric reconstruction of *MonoDepth2* to perform test-time training. This involves unfreezing the depth encoder  $\mathcal{E}$  and the decoder  $\mathcal{T}$  at test time and training them using the loss function described in Section 3.4. (ii) TTT **MAE** uses an additional self-supervision decoder ( $\mathcal{S}$ ) that is placed on top of the encoder ( $\mathcal{E}$ ) to perform the uncertainty-aware masked autoencoding both at training and test-time training as described in Section 3.3 & 3.4. For test-time training, the decoder  $\mathcal{T}$  is frozen. (iii) TTT **orig-SS+MAE** refers to the test-time training method that leverages both the original self-supervision technique in the *MonoDepth2* and the additional decoding head to perform masked autoencoding. At test time, all three networks ( $\mathcal{E}, \mathcal{T}, \mathcal{S}$ ) are unfrozen and trained as described in Section 3.3 & 3.4.

### 4.2 Pre-trained Models on One Domain Perform Poorly on Shifted Domains

Table 1 shows the performance of *MonoDepth2* trained on the KITTI dataset on multiple shifted domains, i.e., “Night” (daytime-to-night), “Foggy” (clear-to-foggy), “Rainy” (clear-to-rainy) as shown in Figure 4. We see that the pre-trained model performs best on the KITTI dataset (similar domain as that of training domain) with Abs Rel of 0.115. However, the performance of the same model on the other shifted domains degrades substantially with Abs Rel of 0.322 on “Night” and 0.301/0.281 on “Foggy”/“Rainy” respectively. Furthermore, we fine-tuned *MonoDepth2* (originally trained on KITTI) on the different SHIFT domains.

We observe that the performance of *MonoDepth2* for a particular domain shift improves substantially when we fine-tune the KITTI-based model on that shifted domain; for instance, the performance of a fine-tuned *MonoDepth2* (with “Night”) on “Night” dataset (and not on train dataset) improves with an **Abs Rel** of 0.263 (compared to 0.322 for non-fine-tuned KITTI-based model). However, the fine-tuned model performs worse on the original KITTI domain (**Abs Rel** of 0.462). We observe a similar trend for other SHIFT domains. This indicates that a model trained on a static dataset when deployed to the real world where it may face continuously shifting domains will suffer, and there is a need for methods that can adapt to shifting distributions on-the-fly.

D	Metrics	Monodepth-2 (KITTI)	Monodepth-2 (“Night”)	Monodepth-2 (“Foggy”)	Monodepth-2 (“Rainy”)
KITTI	Abs Rel↓	<b>0.115</b>	0.462	0.397	0.411
	RMSE↓	<b>4.863</b>	6.259	5.865	6.122
	RMSE log↓	<b>0.193</b>	0.497	0.523	0.561
	$\delta < 1.25 \uparrow$	<b>0.877</b>	0.573	0.536	0.568
	$\delta < 1.25^2 \uparrow$	<b>0.959</b>	0.634	0.614	0.633
	$\delta < 1.25^3 \uparrow$	<b>0.981</b>	0.712	0.672	0.708
“Night”	Abs Rel↓	0.322	<b>0.263</b>	0.299	0.312
	RMSE↓	5.742	<b>5.137</b>	5.672	5.433
	RMSE log↓	0.624	<b>0.295</b>	0.387	0.452
	$\delta < 1.25 \uparrow$	0.522	<b>0.711</b>	0.646	0.632
	$\delta < 1.25^2 \uparrow$	0.720	<b>0.772</b>	0.733	0.754
	$\delta < 1.25^3 \uparrow$	0.814	<b>0.836</b>	0.831	0.822
“Foggy”	Abs Rel↓	0.301	0.288	<b>0.203</b>	0.294
	RMSE↓	7.283	6.972	<b>4.923</b>	6.832
	RMSE log↓	0.796	0.622	<b>0.223</b>	0.654
	$\delta < 1.25 \uparrow$	0.598	0.664	<b>0.749</b>	0.682
	$\delta < 1.25^2 \uparrow$	0.749	0.763	<b>0.836</b>	0.754
	$\delta < 1.25^3 \uparrow$	0.806	0.812	<b>0.882</b>	0.803
“Rainy”	Abs Rel↓	0.281	0.272	0.268	<b>0.197</b>
	RMSE↓	6.681	6.255	6.517	<b>4.611</b>
	RMSE log↓	0.705	0.687	0.662	<b>0.239</b>
	$\delta < 1.25 \uparrow$	0.628	0.693	0.682	<b>0.788</b>
	$\delta < 1.25^2 \uparrow$	0.767	0.753	0.762	<b>0.844</b>
	$\delta < 1.25^3 \uparrow$	0.824	0.833	0.841	<b>0.878</b>

**Table 1:** Comparison showing that *MonoDepth2* performs well (metrics in **bold**) only on the domain it was trained on, i.e., it does not generalize well to data from a shifted domain, indicating the need for online domain adaptation.

### 4.3 Test-Time Training for On-the-fly Domain Adaptation Applied to Dense Prediction

Addressing the limitations highlighted in the previous section, we modify the original *MonoDepth2* to incorporate the test-time training, leading to methods TTT orig-SS, TTT MAE, and TTT orig-SS+MAE as described in Section 3.4 & 4.1. Figure 5 shows the performance of various test-time training techniques on different domains with a varying number of test-time training steps. All the models were pre-trained on KITTI and evaluated on the SHIFT dataset (Sun et al., 2022) with different domain shifts including Daytime-to-Night (“Night”), Clear-to-Foggy (“Foggy”), Clear-to-Rainy (“Rainy”). Table 2 summarizes the performance of all test-time training methods in terms of different performance metrics in various shifted domains. Figure 5 shows that TTT orig-SS+MAE performs the best across all domains. For instance, with “Night”, method TTT orig-SS starts to improve (indicated by lower Abs Rel and RMSE log) as we gradually increase the number of test-time training steps at each frame. It eventually hits the optimal point at close to 16 steps and then performance starts to deteriorate with an increasing number of steps. This phenomenon has been attributed to overfitting in previous works (Gandelsman et al., 2022). While TTT orig-SS leverages the original self-supervision components in *MonoDepth2* to perform test-time training, a similar trend is observed for TTT MAE that leverages the additional head that performs masked-autoencoding (and does not unfreeze the depth



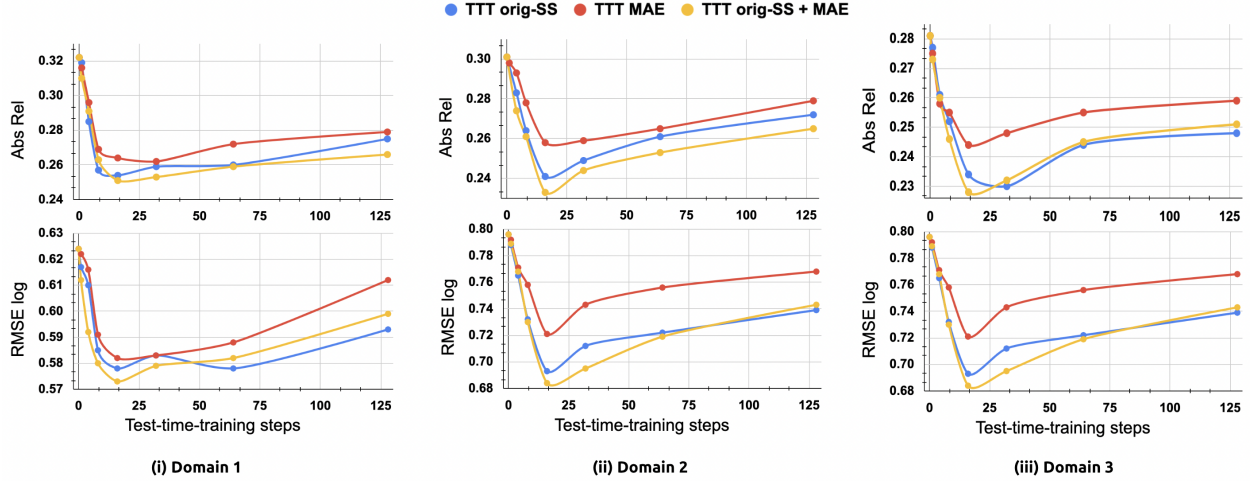


**Figure 5:** Performance (Abs Rel & RMSE Log) vs. number of Test-Time Training steps in different shifted domains for methods TTT orig-SS, TTT MAE, and TTT orig-SS+MAE

D	Methods	Abs Rel ↓	RMSE ↓	RMSE log ↓	$\delta < 1.25 \uparrow$	$\delta < 1.25^2 \uparrow$	$\delta < 1.25^3 \uparrow$
"Night"	<i>Monodepth2</i>	0.322	5.742	0.624	0.522	0.720	0.814
	+ TTT orig-SS	0.254	5.344	0.578	0.643	0.773	0.863
	+ TTT MAE	0.262	5.532	0.582	0.636	0.792	0.895
	+ TTT orig-SS+MAE	<b>0.251</b>	<b>5.216</b>	<b>0.573</b>	<b>0.674</b>	<b>0.811</b>	<b>0.907</b>
"Foggy"	<i>Monodepth2</i>	0.301	7.283	0.796	0.598	0.749	0.806
	+ TTT orig-SS	0.241	6.874	0.693	0.635	0.773	0.833
	+ TTT MAE	0.258	7.033	0.721	0.672	0.761	0.827
	+ TTT orig-SS+MAE	<b>0.233</b>	<b>6.722</b>	<b>0.684</b>	<b>0.717</b>	<b>0.794</b>	<b>0.856</b>
"Rainy"	<i>Monodepth2</i>	0.281	6.681	0.705	0.628	0.767	0.824
	+ TTT orig-SS	0.230	6.293	0.631	0.667	0.783	0.856
	+ TTT MAE	0.244	6.366	0.633	0.655	0.775	0.837
	+ TTT orig-SS+MAE	<b>0.228</b>	<b>6.112</b>	<b>0.618</b>	<b>0.694</b>	<b>0.803</b>	<b>0.886</b>

**Table 2:** Performance comparison for different test-time training techniques on different shifted domains.

decoder head at test-time). However, the best performance is observed with TTT orig-SS+MAE that combines both the original self-supervision and the additional masked-autoencoding-based self-supervision to perform test-time training.

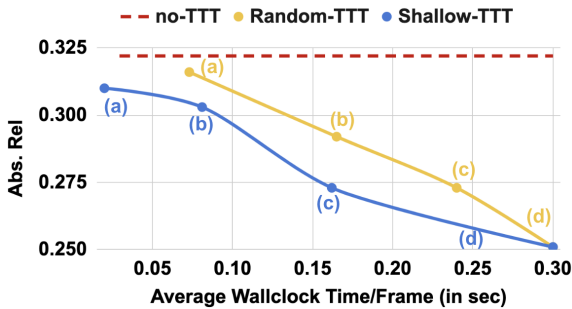


**Figure 6:** Making TTT orig-SS+MAE efficient by (i) applying TTT randomly on some test inputs (Random-TTT), and (ii) Running TTT for less number of steps (shallow-TTT) on all the test inputs coming from the shifted domain ("Night").

chance of preventing expensive test-time training for many input samples leading to a small average wall-

clock time spent per sample, however, the performance gain is also insignificant, compared to no application of TTT as shown with the dashed line. Points (b), (c), and (d) on the **Random-TTT** curve show the results for applying test-time training to each test input randomly with a probability of 50%, 75%, and 100%. As test-time training is applied to more samples, the performance improves but the average wall-clock time spent per sample also increases. To strike an optimal balance between wall-clock time at inference and performance, method **Shallow-TTT** in Figure 6 indicates the application of test-time training for every test input but with less number of steps. Points (a), (b), (c), and (d) indicate the application of test-time training with 2, 4, 8, and 16 steps. While shallow test-time training is faster, it does not lead to large gains in performance.

#### 4.4 Systematically Improving the Efficiency of Test-Time Training

As discussed in previous section, while test-time training improves the performance of monocular depth estimation in the presence of domain shifts, it comes at the cost of increased inference time, making it inefficient and undesirable for real-world applications. Figure 6 suggests that it may be possible to achieve an optimal balance between performance and inference time by selectively applying test-time training and exploiting the continuous nature of domain shift by preserving the state of models between keyframes. While the experiment with **Random-TTT** in Figure 6 randomly applies test-time training to certain samples, we refine it further by applying test-time training to only certain “key” test samples/frames and preserving the state of models between consecutive keyframes. We study the results with a naive strategy and an intelligent strategy to identify “keyframes” to apply TTT. Now, we use **TTT orig-SS+MAE** as our TTT method.

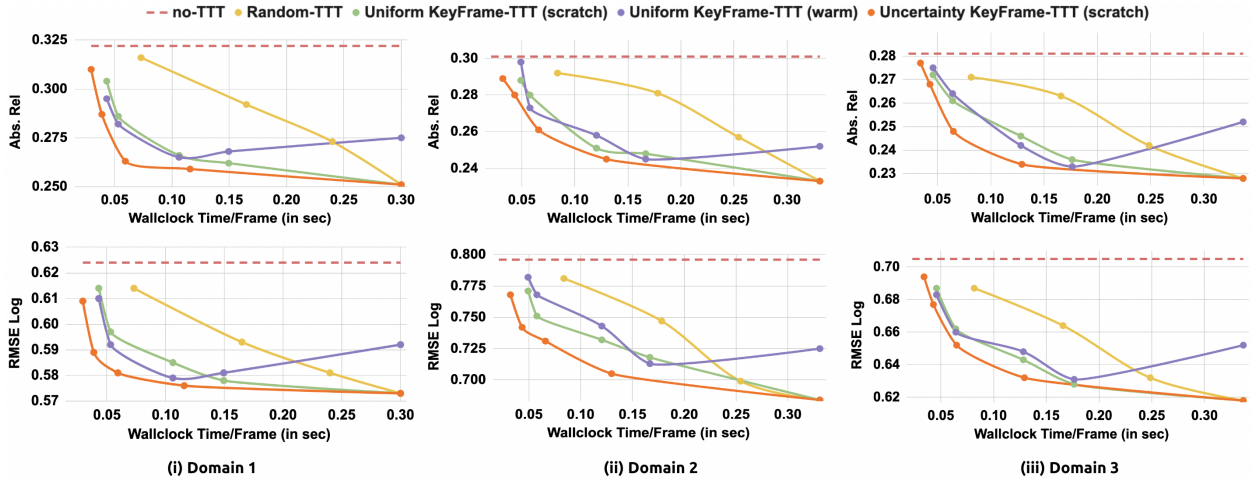


**Figure 7:** Test-Time Training can be made more efficient (i.e., achieving better performance faster) by selectively applying Test-Time Training only to keyframes. These figures visualize the performance for various strategy to identify keyframes as described in Section 4.4.

**Naive Strategy 1 – Uniformly Distributed keyframes (scratch) with preserved states.** In this strategy, we assume that every  $n^{th}$  frame (e.g., every  $10^{th}$  frame) in a stream of inputs is a keyframe, and the intermediate frames between two consecutive keyframes do not change drastically. The standard TTT techniques, where test-time training happens at every frame, is a special case of this naive strategy with  $n = 1$ . Figure 7 shows the results of the experiments for TTT with this strategy for different values of  $n \in \{20, 10, 5, 2, 1\}$ , referred to as **Uniform KeyFrame-TTT (scratch)**. Here (**scratch**) refers to performing TTT at every keyframe starting from the checkpoint of the original source domain. Also, we preserve the state of the models between two consecutive keyframes. We notice that as the value of  $n$  decreases (i.e., TTT is applied to more frames) the performance improves, but the average wallclock time per frame also increases. It can also be observed that this naive strategy performs better than randomly selecting the frames for TTT (i.e., **Random-TTT**). While effective, it assumes that novel keyframes appear uniformly in the stream, which is not true. As a result, when a smaller number of frames is selected for TTT (i.e.,  $n = 20$ ), the gain in performance is not significant (compared to not applying TTT), indicating that a better proxy to identify keyframes may lead to improvements.

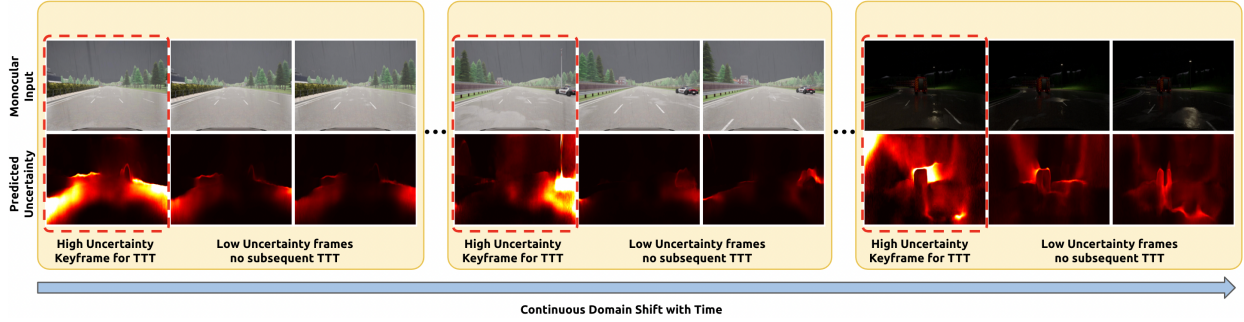


**Figure 8:** Uncertainty-based key-frame identification for selective TTT with state preservation between keyframes (i.e., applying TTT to samples that have higher uncertainty/entropy). From left-to-right stream of inputs (top) with the corresponding uncertainty estimates (bottom). The novel frame has higher entropy and is flagged as a keyframe (red-dashed box). The yellow box shows frames for which model states are preserved.

**Naive Strategy 2 – Uniformly Distributed keyframes (warm) with preserved states.** Similar to *Naive Strategy 1*, this strategy assumes that keyframes are uniformly distributed. However, TTT at any given frame uses the checkpoints from the last TTT frame for initialization (unlike *Naive Strategy 1* that uses the checkpoint trained on the source domain). Figure 7 shows the results of the experiments for TTT with this strategy for different values of  $n \in \{20, 10, 5, 2, 1\}$ , referred to as **Uniform KeyFrame-TTT (warm)**. We notice that in the beginning, as the value of  $n$  decreases (i.e., TTT is applied to more frames), performance improves, but after a point when TTT is applied frequently, performance starts to degrade, indicating that using the previous TTT step checkpoints eventually leads to overfitting.

**Intelligent Strategy – Uncertainty keyframes (scratch) with preserved states.** The above strategies highlight the importance of choosing the right keyframes to apply TTT. The proposed  $UT^3$  framework provides an informative proxy to identify keyframes by quantifying the uncertainty in the reconstructions as described in Section 3.3 & 3.4. Given the associated uncertainty estimates for every input frame, we quantify the entropy of the input frame and compare it with the distribution of entropy values for the samples in the source domain. A threshold for the entropy value is defined using the source SHIFT Distribution. At the test time, samples with higher entropy are flagged as keyframes for TTT.

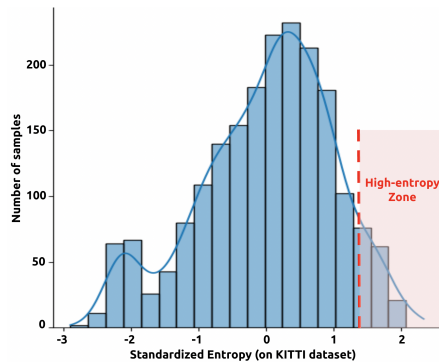


**Figure 9:** Entropy distribution derived from TTT orig-SS+MAE.

Figure 9 shows the distribution of standardized entropy values (i.e., entropy  $\kappa$  is transformed to  $\frac{\kappa - \bar{\kappa}_s}{\sqrt{\mathcal{V}_{\kappa,s}}}$ , where  $\bar{\kappa}_s$  is the mean and  $\mathcal{V}_{\kappa,s}$  the variance of all entropy values in source domain) for the samples in source domain that we obtain from the trained TTT orig-SS+MAE method. It also shows the threshold that is set at the  $q\%$ -tile beyond which is the high-entropy zone (shown in red) where the frames will be flagged as keyframes and TTT will be performed. Figure 8 shows a qualitative example of the processing of input frames (belonging to “Night”) at the test time. It indicates that novel frames (Figure 8-top row), when first encountered, have high uncertainty values (shown in bright colors, which translates to high entropy) produced by the self-supervision head that performs uncertainty-aware masked-autoencoding (Figure 8-bottom row). These novel frames are selected as keyframes. After completing TTT on a keyframe, the subsequent frames have lower uncertainty estimates (hence lower entropy) and do not get flagged as key-frame for TTT until the next novel input frame appears. Figure 7 shows results for this strategy (**Uncertainty keyframes (scratch)**) with different entropy thresholds (a higher threshold leads to less number of keyframes) in comparison to other strategies. We observe that uncertainty-based key-frame identification can achieve the best performance  $\approx 70\%$  faster across all the domains.

---

## 5 Discussion and Conclusion

In this work, we presented a novel framework named UT<sup>3</sup> that performs efficient test-time training. The proposed method leverages an uncertainty-aware self-supervision task to quantify the uncertainty (and the entropy) at test time, allowing for the selective application of test-time training. The selective application of test-time training leads to substantial improvements in inference time, making it suitable for applications where limited computing resources and high latency are often tight constraints. We demonstrated the effectiveness of our method on monocular depth estimation. Our experiments study various strategies using test-time training and show that the proposed method improves the latency-performance trade-off of test-time training in the presence of test data from shifted domains. Our method allows autonomous systems to adapt better to changing environments while reducing the computational burden on the system. The proposed UT<sup>3</sup> framework offers a promising solution to the challenge of adapting to continuously evolving environments in autonomous systems by offering a lever to find the right test-time training setup that allows a trade-off between performance and computational efficiency, making it suitable for real-world applications. We believe that this work will pave the way for further advancements in the field of test-time training and provide a more efficient approach for autonomous systems to handle the dynamic nature of the real world.

## References

- Abdullah A Abdullah, Masoud M Hassan, and Yaseen T Mustafa. A review on bayesian deep learning in healthcare: Applications and challenges. *IEEE Access*, 2022.
- Fatemeh Azimi, Sebastian Palacio, Federico Raue, Jörn Hees, Luca Bertinetto, and Andreas Dengel. Self-supervised test-time adaptation on video data. In *Proceedings of the IEEE/CVF Winter Conference on Applications of Computer Vision*, pp. 3439–3448, 2022.
- Shai Ben-David, John Blitzer, Koby Crammer, Alex Kulesza, Fernando Pereira, and Jennifer Wortman Vaughan. A theory of learning from different domains. *Machine learning*, 79:151–175, 2010.
- John Blitzer, Ryan McDonald, and Fernando Pereira. Domain adaptation with structural correspondence learning. In *Proceedings of the 2006 conference on empirical methods in natural language processing*, pp. 120–128, 2006.
- John Bridle and Stephen J Cox. Recnorm: Simultaneous normalisation and classification applied to speech recognition. *Advances in Neural Information Processing Systems*, 3, 1990.
- Liang-Chieh Chen, George Papandreou, Iasonas Kokkinos, Kevin Murphy, and Alan L Yuille. Deeplab: Semantic image segmentation with deep convolutional nets, atrous convolution, and fully connected crfs. *IEEE transactions on pattern analysis and machine intelligence*, 40(4):834–848, 2017.
- Gabriela Csurka. A comprehensive survey on domain adaptation for visual applications. *Domain adaptation in computer vision applications*, pp. 1–35, 2017.
- Erik Daxberger, Agustinus Kristiadi, Alexander Immer, Runa Eschenhagen, Matthias Bauer, and Philipp Hennig. Laplace redux-effortless bayesian deep learning. *NeurIPS*, 2021.
- Jun Deng, Xinzhou Xu, Zixing Zhang, Sascha Frühholz, and Björn Schuller. Universum autoencoder-based domain adaptation for speech emotion recognition. *IEEE Signal Processing Letters*, 24(4):500–504, 2017.
- Nikita Durasov, Timur Bagautdinov, Pierre Baque, and Pascal Fua. Masksembles for uncertainty estimation. In *Proceedings of the IEEE/CVF Conference on Computer Vision and Pattern Recognition*, pp. 13539–13548, 2021.
- Fatima El Jamiy and Ronald Marsh. Survey on depth perception in head mounted displays: distance estimation in virtual reality, augmented reality, and mixed reality. *IET Image Processing*, 13(5):707–712, 2019.

- 
- Basura Fernando, Amaury Habrard, Marc Sebban, and Tinne Tuytelaars. Unsupervised visual domain adaptation using subspace alignment. In *Proceedings of the IEEE international conference on computer vision*, pp. 2960–2967, 2013.
- Huan Fu, Mingming Gong, Chaohui Wang, Kayhan Batmanghelich, and Dacheng Tao. Deep ordinal regression network for monocular depth estimation. In *Proceedings of the IEEE conference on computer vision and pattern recognition*, pp. 2002–2011, 2018.
- Yarin Gal. Uncertainty in deep learning. 2016.
- Yossi Gandelsman, Yu Sun, Xinlei Chen, and Alexei A Efros. Test-time training with masked autoencoders. In *Advances in Neural Information Processing Systems*, 2022.
- Yaroslav Ganin, Evgeniya Ustinova, Hana Ajakan, Pascal Germain, Hugo Larochelle, François Laviolette, Mario Marchand, and Victor Lempitsky. Domain-adversarial training of neural networks. *The journal of machine learning research*, 17(1):2096–2030, 2016.
- Andreas Geiger, Philip Lenz, and Raquel Urtasun. Are we ready for autonomous driving? the kitti vision benchmark suite. In *Conference on Computer Vision and Pattern Recognition (CVPR)*, 2012.
- Clément Godard, Oisín Mac Aodha, and Gabriel J Brostow. Unsupervised monocular depth estimation with left-right consistency. In *Proceedings of the IEEE conference on computer vision and pattern recognition*, pp. 270–279, 2017.
- Clément Godard, Oisín Mac Aodha, Michael Firman, and Gabriel J Brostow. Digging into self-supervised monocular depth estimation. In *Proceedings of the IEEE/CVF international conference on computer vision*, pp. 3828–3838, 2019.
- Fredrik K Gustafsson, Martin Danelljan, and Thomas B Schon. Evaluating scalable bayesian deep learning methods for robust computer vision. In *Proceedings of the IEEE/CVF conference on computer vision and pattern recognition workshops*, pp. 318–319, 2020.
- Fa-Ting Hong, Longhao Zhang, Li Shen, and Dan Xu. Depth-aware generative adversarial network for talking head video generation. In *Proceedings of the IEEE/CVF Conference on Computer Vision and Pattern Recognition*, pp. 3397–3406, 2022.
- Yusuke Iwasawa and Yutaka Matsuo. Test-time classifier adjustment module for model-agnostic domain generalization. *Advances in Neural Information Processing Systems*, 34:2427–2440, 2021.
- Jing Jiang and ChengXiang Zhai. Instance weighting for domain adaptation in nlp. *ACL*, 2007.
- Alex Kendall and Yarin Gal. What uncertainties do we need in bayesian deep learning for computer vision? *NIPS*, 2017.
- Diederik P Kingma and Jimmy Ba. Adam: A method for stochastic optimization. *arXiv preprint arXiv:1412.6980*, 2014.
- Pang Wei Koh, Shiori Sagawa, Henrik Marklund, Sang Michael Xie, Marvin Zhang, Akshay Balsubramani, Weihua Hu, Michihiro Yasunaga, Richard Lanus Phillips, Irena Gao, et al. Wilds: A benchmark of in-the-wild distribution shifts. In *International Conference on Machine Learning*, pp. 5637–5664. PMLR, 2021.
- Varun Ravi Kumar, Stefan Milz, Christian Witt, Martin Simon, Karl Amende, Johannes Petzold, Senthil Yogamani, and Timo Pech. Near-field depth estimation using monocular fisheye camera: A semi-supervised learning approach using sparse lidar data. In *CVPR Workshop*, volume 7, pp. 2, 2018.
- Balaji Lakshminarayanan, Alexander Pritzel, and Charles Blundell. Simple and scalable predictive uncertainty estimation using deep ensembles. *arXiv preprint arXiv:1612.01474*, 2016.



- 
- Siddique Latif, Rajib Rana, Sara Khalifa, Raja Jurdak, and Bjorn Wolfgang Schuller. Self supervised adversarial domain adaptation for cross-corpus and cross-language speech emotion recognition. *IEEE Transactions on Affective Computing*, 2022.
- Max-Heinrich Laves, Sontje Ihler, Jacob F Fast, Lüder A Kahrs, and Tobias Ortmaier. Well-calibrated regression uncertainty in medical imaging with deep learning. In *Medical Imaging with Deep Learning*, pp. 393–412. PMLR, 2020a.
- Max-Heinrich Laves, Sontje Ihler, Karl-Philipp Kortmann, and Tobias Ortmaier. Calibration of model uncertainty for dropout variational inference. *arXiv preprint arXiv:2006.11584*, 2020b.
- Wei Lin, Muhammad Jehanzeb Mirza, Mateusz Kozinski, Horst Possegger, Hilde Kuehne, and Horst Bischof. Video test-time adaptation for action recognition. *arXiv preprint arXiv:2211.15393*, 2022.
- Chenxi Liu, Lixu Wang, Lingjuan Lyu, Chen Sun, Xiao Wang, and Qi Zhu. Deja vu: Continual model generalization for unseen domains. *arXiv preprint arXiv:2301.10418*, 2023.
- Dongnan Liu, Donghao Zhang, Yang Song, Fan Zhang, Lauren O’Donnell, Heng Huang, Mei Chen, and Weidong Cai. Unsupervised instance segmentation in microscopy images via panoptic domain adaptation and task re-weighting. In *Proceedings of the IEEE/CVF conference on computer vision and pattern recognition*, pp. 4243–4252, 2020.
- Yuejiang Liu, Parth Kothari, Bastien Van Delft, Baptiste Bellot-Gurlet, Taylor Mordan, and Alexandre Alahi. Ttt++: When does self-supervised test-time training fail or thrive? *Advances in Neural Information Processing Systems*, 34:21808–21820, 2021.
- Andrey Malinin and Mark Gales. Predictive uncertainty estimation via prior networks. *Advances in neural information processing systems*, 31, 2018.
- Yishay Mansour, Mehryar Mohri, and Afshin Rostamizadeh. Domain adaptation with multiple sources. *Advances in neural information processing systems*, 21, 2008.
- Yue Ming, Xuyang Meng, Chunxiao Fan, and Hui Yu. Deep learning for monocular depth estimation: A review. *Neurocomputing*, 438:14–33, 2021.
- Theodoros Panagiotakopoulos, Pier Luigi Dovesi, Linus Härenstam-Nielsen, and Matteo Poggi. Online domain adaptation for semantic segmentation in ever-changing conditions. In *Computer Vision–ECCV 2022: 17th European Conference, Tel Aviv, Israel, October 23–27, 2022, Proceedings, Part XXXIV*, pp. 128–146. Springer, 2022.
- Kihong Park, Seungryong Kim, and Kwanghoon Sohn. High-precision depth estimation using uncalibrated lidar and stereo fusion. *Ieee transactions on intelligent transportation systems*, 21(1):321–335, 2019.
- Vaishakh Patil, Christos Sakaridis, Alexander Liniger, and Luc Van Gool. P3depth: Monocular depth estimation with a piecewise planarity prior. In *Proceedings of the IEEE/CVF Conference on Computer Vision and Pattern Recognition*, pp. 1610–1621, 2022.
- Alan Ramponi and Barbara Plank. Neural unsupervised domain adaptation in nlp—a survey. *arXiv preprint arXiv:2006.00632*, 2020.
- Vikrant Rangnekar, Uddeshya Upadhyay, Zeynep Akata, and Biplab Banerjee. Usim-dal: Uncertainty-aware statistical image modeling-based dense active learning for super-resolution. *arXiv preprint arXiv:2305.17520*, 2023.
- Tom Roussel, Luc Van Eycken, and Tinne Tuytelaars. Monocular depth estimation in new environments with absolute scale. In *2019 IEEE/RSJ International Conference on Intelligent Robots and Systems (IROS)*, pp. 1735–1741. IEEE, 2019.
- Alexander Shapeev, Konstantin Gubaev, Evgenii Tsymbalov, and Evgeny Podryabinkin. Active learning and uncertainty estimation. *Machine Learning Meets Quantum Physics*, pp. 309–329, 2020.

- 
- Viswanath P Sudarshan, Uddeshya Upadhyay, Gary F Egan, Zhaolin Chen, and Suyash P Awate. Towards lower-dose PET using physics-based uncertainty-aware multimodal learning with robustness to out-of-distribution data. *Medical Image Analysis*, 2021.
- Shiliang Sun, Honglei Shi, and Yuanbin Wu. A survey of multi-source domain adaptation. *Information Fusion*, 24:84–92, 2015.
- Tao Sun, Mattia Segu, Janis Postels, Yuxuan Wang, Luc Van Gool, Bernt Schiele, Federico Tombari, and Fisher Yu. SHIFT: a synthetic driving dataset for continuous multi-task domain adaptation. In *Proceedings of the IEEE/CVF Conference on Computer Vision and Pattern Recognition (CVPR)*, pp. 21371–21382, June 2022.
- Yu Sun, Xiaolong Wang, Zhuang Liu, John Miller, Alexei Efros, and Moritz Hardt. Test-time training with self-supervision for generalization under distribution shifts. In *International conference on machine learning*, pp. 9229–9248. PMLR, 2020.
- Yuan Tian, Ruihao Yuan, Dezhen Xue, Yumei Zhou, Xiangdong Ding, Jun Sun, and Turab Lookman. Role of uncertainty estimation in accelerating materials development via active learning. *Journal of Applied Physics*, 128(1):014103, 2020.
- Uddeshya Upadhyay, Yanbei Chen, and Zeynep Akata. Robustness via uncertainty-aware cycle consistency. *NeurIPS*, 2021a.
- Uddeshya Upadhyay, Yanbei Chen, Tobias Hepp, Sergios Gatidis, and Zeynep Akata. Uncertainty-guided progressive gans for medical image translation. In *MICCAI*, 2021b.
- Uddeshya Upadhyay, Viswanath P Sudarshan, and Suyash P Awate. Uncertainty-aware GAN with adaptive loss for robust mri image enhancement. In *IEEE ICCV Workshop*, 2021c.
- Uddeshya Upadhyay, Shyamgopal Karthik, Yanbei Chen, Massimiliano Mancini, and Zeynep Akata. BayesCap: Bayesian identity cap for calibrated uncertainty in frozen neural networks. In *European Conference on Computer Vision*, pp. 299–317. Springer, 2022.
- Uddeshya Upadhyay, Sairam Bade, Arjun Puranik, Shahir Asfahan, Melwin Babu, Francisco Lopez-Jimenez, Samuel J Asirvatham, Ashim Prasad, Ajit Rajasekharan, Samir Awasthi, et al. Hypuc: Hyperfine uncertainty calibration with gradient-boosted corrections for reliable regression on imbalanced electrocardiograms. *arXiv preprint arXiv:2311.13821*, 2023a.
- Uddeshya Upadhyay, Shyamgopal Karthik, Massimiliano Mancini, and Zeynep Akata. Problm: Probabilistic adapter for frozen vision-language models. In *Proceedings of the IEEE/CVF International Conference on Computer Vision*, pp. 1899–1910, 2023b.
- Uddeshya Upadhyay, Jae Myung Kim, Cordelia Schmidt, Bernhard Schölkopf, and Zeynep Akata. Likelihood annealing: Fast calibrated uncertainty for regression. *arXiv preprint arXiv:2302.11012*, 2023c.
- Chaoyang Wang, José Miguel Buenaposada, Rui Zhu, and Simon Lucey. Learning depth from monocular videos using direct methods. In *Proceedings of the IEEE conference on computer vision and pattern recognition*, pp. 2022–2030, 2018.
- Dequan Wang, Evan Shelhamer, Shaoteng Liu, Bruno Olshausen, and Trevor Darrell. Tent: Fully test-time adaptation by entropy minimization. *arXiv preprint arXiv:2006.10726*, 2020a.
- Guotai Wang, Wenqi Li, Michael Aertsen, Jan Deprest, Sébastien Ourselin, and Tom Vercauteren. Aleatoric uncertainty estimation with test-time augmentation for medical image segmentation with convolutional neural networks. *Neurocomputing*, 338:34–45, 2019.
- Hang Wang, Minghao Xu, Bingbing Ni, and Wenjun Zhang. Learning to combine: Knowledge aggregation for multi-source domain adaptation. In *Computer Vision–ECCV 2020: 16th European Conference, Glasgow, UK, August 23–28, 2020, Proceedings, Part VIII 16*, pp. 727–744. Springer, 2020b.

- 
- Hao Wang and Dit-Yan Yeung. A survey on bayesian deep learning. *ACM computing surveys (csur)*, 53(5): 1–37, 2020.
- Mei Wang and Weihong Deng. Deep visual domain adaptation: A survey. *Neurocomputing*, 312:135–153, 2018.
- Qin Wang, Olga Fink, Luc Van Gool, and Dengxin Dai. Continual test-time domain adaptation. In *Proceedings of the IEEE/CVF Conference on Computer Vision and Pattern Recognition*, pp. 7201–7211, 2022.
- Renhao Wang, Yu Sun, Yossi Gandelsman, Xinlei Chen, Alexei A Efros, and Xiaolong Wang. Test-time training on video streams.
- Andrew G Wilson and Pavel Izmailov. Bayesian deep learning and a probabilistic perspective of generalization. *Advances in neural information processing systems*, 33:4697–4708, 2020.
- Menglong Ye, Edward Johns, Ankur Handa, Lin Zhang, Philip Pratt, and Guang-Zhong Yang. Self-supervised siamese learning on stereo image pairs for depth estimation in robotic surgery. *arXiv preprint arXiv:1705.08260*, 2017.
- Wei Zhang, Xiang Li, Hui Ma, Zhong Luo, and Xu Li. Open-set domain adaptation in machinery fault diagnostics using instance-level weighted adversarial learning. *IEEE Transactions on Industrial Informatics*, 17(11):7445–7455, 2021.
- Yizhe Zhang, Shubhankar Borse, Hong Cai, and Fatih Porikli. Auxadapt: Stable and efficient test-time adaptation for temporally consistent video semantic segmentation. In *Proceedings of the IEEE/CVF Winter Conference on Applications of Computer Vision*, pp. 2339–2348, 2022.
- Shanshan Zhao, Huan Fu, Mingming Gong, and Dacheng Tao. Geometry-aware symmetric domain adaptation for monocular depth estimation. In *Proceedings of the IEEE/CVF Conference on Computer Vision and Pattern Recognition*, pp. 9788–9798, 2019.
- Kaiyang Zhou, Ziwei Liu, Yu Qiao, Tao Xiang, and Chen Change Loy. Domain generalization: A survey. *IEEE Transactions on Pattern Analysis and Machine Intelligence*, 2022.